ACS APPLIED MATERIALS & INTERFACES

www.acsami.org
Research Article

Yoda1-Loaded Microfibrous Scaffolds Accelerate Osteogenesis through Piezo1-F-Actin Pathway-Mediated YAP Nuclear Localization and Functionalization

Junzheng Liu,[†] Zijie Meng,[†] Jidong Song, Jiaming Yu, Qin Guo, Jiahao Zhang, Shuo Wang, Yulin Wang, Zhennan Qiu, Xinyi Zhang, Jiankang He,* and Wei Wang*

Cite This: ACS Appl. Mater. Interfaces 2025, 17, 30559−30572

Read Online

ACCESS | Metrics & More | Article Recommendations | Supporting Information

ABSTRACT: Yoda1 has been recognized as an effective pharmacological intervention for the treatment of critical bone defects. However, the local delivery strategy of Yoda1 is uncommon, and the underlying mechanism through which Yoda1 enhances osteogenesis has been poorly investigated. Here, we propose utilizing electrohydrodynamic (EHD)-printed microfibrous scaffolds as a drug carrier for loading Yoda1 through a polydopamine (PDA) coating, and the synthetic mechanisms for enhancing bone regeneration are explored. Yoda1 was successfully loaded on the surface of the EHD-printed microfibrous scaffolds with the assistance of PDA. The results of *in vitro* experiments demonstrated that the Yoda1-loaded microfibrous scaffold group exhibited a more than 2-fold increase in COL-I protein levels compared to the control group. Additionally, the expression levels of osteogenic indicators such as ALP, Runx2, and OCN genes were significantly increased by 2−4-fold compared to those in the control group. We revealed that Yoda1 can effectively activate the Piezo1-F-actin pathway, thereby facilitating YAP nucleation and promoting lysine histone acetylation. Consequently, this mechanism enhanced the functionality of YAP nucleation and upregulated the expression of COL-I. Moreover, when implanted *in vivo*, the Yoda1-loaded microfibrous scaffold group could promote macrophage M2 polarization, thereby enhancing bone regeneration at defect sites. It is believed that the localized release of Yoda1 via EHD-printed PCL scaffolds might represent a promising strategy for the clinically precise treatment of bone defects.

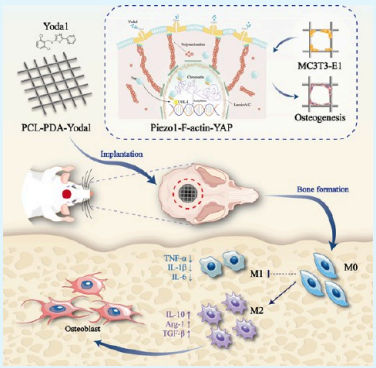

KEYWORDS: *Yoda1, electrohydrodynamic printing, Piezo1, YAP, osteogenesis, bone regeneration*

1. INTRODUCTION

Critical bone defects resulting from trauma, severe infections, or bone tumors often fail to heal through autologous repair, which pose significant global health and economic challenges.[1,2] In recent years, the activation of the mechanically sensitive ion channel protein Piezo1 through mechanical stimulation has been demonstrated to play a pivotal role in the process of bone defect repair.[3−5] For instance, various mechanical stimuli such as fluid shear, low-intensity pulsed ultrasound, and hydrostatic pressure have been employed to activate Piezo1 and facilitate osteogenesis.[6−9] However, applying mechanical stimulation to bone defect areas poses unnecessary risks and practical challenges, including pain sensitivity at the injury site, increased susceptibility to secondary infections, and reliance on external therapeutic devices. These limitations underscore the urgent need to develop alternative approaches for activating Piezo1-mediated mechanotransduction to promote bone regeneration without an external mechanical input.

As an alternative approach for Piezo1 activation, the drug Yoda1 is a known selective agonist capable of activating Piezo1 independently of mechanical stimuli, and its osteogenic effects have been partially confirmed *in vivo*.[10,11] However, because Piezo1 is expressed and functions in a variety of tissues and cells, including cardiovascular tissues, gastrointestinal tissues, chondrocytes, and macrophages, adverse reactions such as overactivation of other tissues and cartilage damage may occur as a result of the current systemic administration of the drug.[12−16] Therefore, a preferred approach would involve the localized delivery of Yoda1 to the specific defect site to target and activate Piezo1 for bone regeneration. In this term, He et al.[17] integrated Yoda1-pretreated bone marrow-derived mesenchymal stem cell exosomes (Exo-Yoda1) into gelatin methacryloyl (GelMA) hydrogels for the treatment of bone defects. The Exo-Yoda1-loaded hydrogel exhibited enhanced osteogenesis in a rat skull bone defect model. In another study,[18] a bilayer membrane loaded with Yoda1 and composed of vertically aligned poly(lactic-*co*-glycolic acid) fibers was electrospun to achieve

Received: February 14, 2025
Revised: April 30, 2025
Accepted: May 2, 2025
Published: May 16, 2025

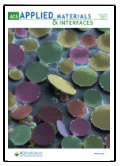

https://doi.org/10.1021/acsami.5c03093
ACS Appl. Mater. Interfaces 2025, 17, 30559−30572

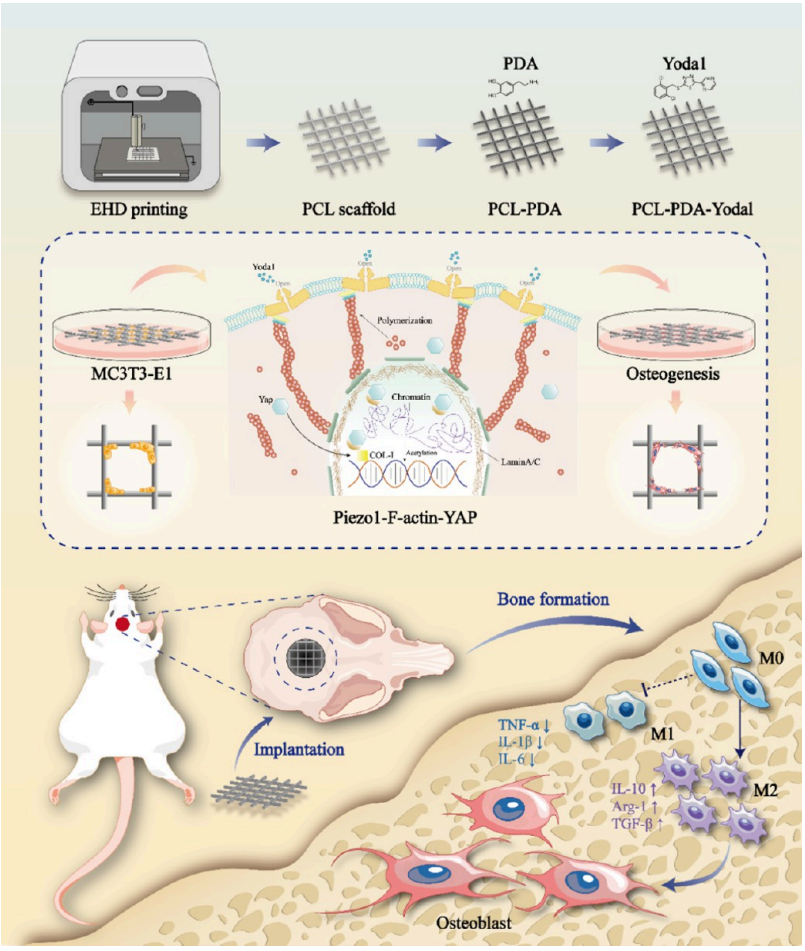

Figure 1. Schematic illustration of the fabrication process for Yoda1-loaded PCL microfibrous scaffolds and their impact on enhancing *in vitro* osteogenic differentiation and *in vivo* osteogenesis.

localized delivery of Yoda1 at the site of the bone defect. This approach demonstrated the effective induction of osseointegration and angiogenesis through controlled release of Yoda1 from the membrane. While the efficacy of Yoda1 in promoting osteogenesis has been demonstrated by these studies, the reliance on exosome engineering or complex membrane fabrication may incur high costs and technical challenges, limiting clinical applicability. Moreover, the soft or ultrathin nature of these carriers may compromise the mechanical stability and cell support during bone regeneration. In this regard, electrohydrodynamic (EHD) printing is a cutting-edge 3D printing technology for the fabrication of drug-loaded tissue engineering scaffolds that has gained widespread acclaim due to its high resolution, capability to modulate cell behaviors, simplicity, and cost-effectiveness.[19−23] Polycaprolactone (PCL) is one of the most widely used and clinically available biopolymers for EHD printing,[24] which has been used for the fabrication of bone tissue engineering scaffolds with enhanced bioactivity.[25,26] To load drug compounds, polydopamine (PDA) coating was reported to be an effective method as PDA has abundant functional groups, such as carboxyl, amino, and imino groups.[27,28] Therefore, the adhesion of Yoda1 onto the EHD-printed scaffolds via PDA coating might be a promising way to simultaneously exert respective superiorities from both microfibrous scaffolds and Yoda1 to promote bone regeneration.

In addition to the necessity of developing local drug delivery strategies, there is still a limited understanding regarding the conversion of chemical signals into osteogenesis-related signals following activation of the Piezo1 channel by Yoda1, as well as how Yoda1 impacts the immune microenvironment for *in vivo* bone regeneration.[18] Although the previous literature has demonstrated that activation of Piezo1 channels can promote osteogenesis by affecting the subcellular localization of Yes-associated protein (YAP), a transcription factor negatively regulated by the Hippo pathway, which is important for cellular proliferation and differentiation.[29−32] However, the mechanism by which Piezo1 regulates the nuclear localization and function of YAP in osteoblasts remains unclear.

In this study, microlattice PCL fibrous scaffolds were fabricated by using EHD printing and subsequently loaded with Yoda1 through PDA coating and adhesion (Figure 1). The osteogenic inductive potential of the Yoda1-loaded microfibrous scaffolds was confirmed through *in vitro* experiments including alkaline phosphatase (ALP) staining and Alizarin Red S (ARS) staining. Furthermore, immunofluorescence staining was performed to assess the levels and distribution of F-actin and YAP, with the results demonstrating the ability of the Yoda1-loaded microfibrous scaffolds to enhance osteogenesis by activating the Piezo1-F-actin pathway and promoting YAP nucleation and function. The impact on the osteogenic immune microenvironment as well as the capacity of the Yoda1-loaded

https://doi.org/10.1021/acsami.5c03093
ACS Appl. Mater. Interfaces 2025, 17, 30559−30572

microfibrous scaffolds to promote new bone generation was further validated *in vivo*.

2. MATERIALS AND METHODS

2.1. Materials. Medical-grade PCL was purchased from Jinan Daigang Biomaterial Co., Ltd. (Mw = 80 000 g/mol, China). Yoda1, TrizmaO hydrochloride, and 3-hydroxytyramine hydrochloride (dopamine hydrochloride) were purchased from Sigma-Aldrich (USA).

2.2. Preparation and PDA Coating of PCL Microfibrous Scaffolds. Microfibrous PCL scaffolds were fabricated using EHD printing (Shaanxi Baipusheng Medical Technology Company, China) with a 300 μm spacing and 90° staggering angle. For EHD printing, the PCL particles were first placed into a glass syringe, and the temperature was set to 80° to melt the particles and form a homogeneous molten mass. Subsequently, indium tin oxide (ITO) glass was selected as the collection substrate, and the PCL scaffolds were printed by employing a nozzle with a size of 20 G, setting a feed rate of 30 μL/h, a voltage of 4.3 kV, and a moving stage at a speed of 30 mm/s, keeping the nozzle-to-substrate distance at a constant of 5 mm during the process.[23] After printing, the PCL scaffolds were placed in a solution containing tris (hydroxymethyl) aminomethane (Tris), and 2 mM dopamine, at a pH of 8.5. To form a homogeneous PDA coating, the scaffolds were placed on a shaker at 25 °C and shaken for 24 h. Following this, the scaffolds were rinsed three times using distilled water for 5 min each time to remove unattached PDA. The PDA-coated PCL scaffolds were then soaked in a Yoda1 solution for 24 h, and the scaffolds were washed at the end of the reaction. For clarity in subsequent descriptions, the untreated pure PCL scaffolds are denoted as the "P" group, the PDA-coated PCL scaffolds are denoted as the "PP" group, and the PDA-coated and Yoda1-loaded PCL scaffolds are denoted as the "PPY" group.

2.3. Structural, Compositional, and Cytocompatibility Analysis of Yoda1-Loaded Scaffolds. The microstructures of the microfibrous scaffolds in the "P" group, "PP" group, and the "PPY" group were examined using scanning electron microscopy (SEM, SU8010, Hitachi, Japan). To further investigate the elemental composition, energy-dispersive spectroscopy (EDS, Vario EL cube, Elementar, Germany) was employed. The surface morphology and roughness of these scaffolds were then assessed by using atomic force microscopy (AFM, Dimension Icon, Bruker, USA). X-ray diffraction (XRD, D8 Advance, Germany) was used to characterize the crystal structures of the scaffolds from different groups. Additionally, the tensile properties of these scaffolds were measured with a universal mechanical testing machine (ETM 103A).

Yoda1 with different concentrations was screened based on the half-maximal inhibitory concentration (IC50) values to evaluate cytotoxicity and identify optimal concentrations. Briefly, MC3T3-E1 (ATCC) was seeded onto the scaffolds with Yoda1 at different concentrations in α-Minimum Essential Medium (α-MEM, Biological Industries, Israel) at a density of 5×10^4 cells per scaffold. After 1, 3, and 5 days of culture, the medium was removed, the cells were washed three times with PBS, and a complete culture medium containing 10% CCK-8 was added. After incubation for 2 h, the culture medium was transferred to 96-well cell culture plates at 100 μL/well, and absorbance was detected by using an enzyme labeler at 450 nm.

To determine the release of Yoda1 from the EHD-printed scaffolds, the scaffolds were immersed into 24-well plates containing 1 mL of PBS and then placed in a 37° constant temperature incubator, and the buffer in the 24-well plates was collected every 2 days and replaced with fresh PBS. A microplate spectrophotometer (BioTek Instruments Inc., USA) was used to measure the Yoda1 concentration to form a release curve.

2.4. Osteogenic Differentiation of MC3T3-E1 on the Yoda1-Loaded Microfibrous Scaffolds. Collagen I (COL-I) immunofluorescence staining, ALP, and ARS staining were performed on cell-laden P scaffolds, PP scaffolds, and PPY scaffolds to investigate the effects of PDA and Yoda1 on osteoblast differentiation. In addition, to investigate the impact of Yoda1 on macrophages and its influence on the osteogenic differentiation of MC3T3-E1, Yoda1-loaded scaffolds were cocultured with RAW 264.7 in Dulbecco'smodified Eagle medium (DMEM, Gibco, USA) supplemented with 10% fetal bovine serum (Biological Industries, Israel) for 3 days, and their supernatants were collected. The supernatant was mixed in a 1:1 ratio with a fresh α-MEM medium to obtain a new conditioned medium, and then MC3T3-E1 cells on the scaffolds of the PPY group were incubated with this medium and named the "PPY+RAW" group.

The osteogenic differentiation of MC3T3-E1 cells on the scaffolds of the four groups was analyzed by COL-I immunofluorescence staining. On day 3 after cell inoculation, the cells were fixed in 4% paraformaldehyde after removing the culture medium and washing with PBS. Afterward, the cell-scaffold complexes were permeabilized with 0.25% Triton X-100, blocked with 3% BSA, and then incubated overnight at 4° with primary COL-I antibody (Affinity, AF5122). Then, after removing the primary antibody, the samples were incubated with Alexa Fluor 647-conjugated antirabbit IgG H&L (Wuhan, China) for 60 min, washed, and then stained with DAPI for 5 min. COL-I was visualized using a laser confocal microscope (A1, Nikon, Japan) and analyzed using the ImageJ software for quantitative analysis of COL-I.

ALP staining was also performed on four groups using the BCIP/NBT ALP color development kit (Beyotime, China) according to the manufacturer's instructions. Briefly, each group was rinsed, fixed, and then incubated in a BCIP/NBT solution for 30 min. Afterward, ALP activity was measured on the four newly cultured groups of cells. Collecting the supernatant, cells were lysed from the scaffolds on ice with RIPA lysis buffer (Beyotime, China), and the amount of converted *p*-nitrophenol was measured by using the *p*-nitrophenyl phosphate (PNPP) assay. A bicinchoninic acid protein assay kit (BCA, Beyotime, China) was used to calibrate the protein concentration to standardize the ALP activity of MC3T3-E1 cells, while calcium deposition was observed by staining scaffolds from all four groups with an ARS kit at 21 and 28 days.

Quantitative real-time polymerase chain reaction (qRT-PCR) was further used to quantify the expression of osteogenesis-related genes of COL-I, ALP, OCN, and Runx2. Specifically, total RNA was extracted from each group of scaffold cells using the Trizol reagent (Invitrogen, USA), centrifuged, and treated with DEPC to measure its concentration. Reverse transcription was performed by a reverse transcription kit (Takara, Dalian, China) and amplified by a SYBR Taq Kit (Takara, Dalian, China). Glyceraldehyde 3-phosphate dehydrogenase (GAPDH) served as an internal reference. Primer sequences are detailed in Table S1.

2.5. Characterization of YAP Nuclear Localization. To investigate the process of Yoda1-loaded PCL scaffolds in activating the Piezo1-F-actin pathway in MC3T3-E1 cells, immunofluorescence and qRT-PCR assays were conducted on the MC3T3-E1 cells seeded on P, PP, and PPY scaffolds. The immunofluorescence staining procedure and qRT-PCR were the same as those described above. The primary antibodies used in this study are listed in Table S2. The ratiometric dye Fluo-4 AM was used to label the cytoplasmic Ca^{2+} concentration, and the calcium fluorescence intensity of the stained samples was detected by laser confocal microscopy. The fluorescence intensity of the stained samples was quantitatively analyzed using image J for all groups. Moreover, SEM was also employed for the observation of the cell morphology.

To investigate the effect of the Pizoe1-F-actin pathway on YAP nuclear localization, we used immunofluorescence staining. Moreover, to further determine the effect of F-actin on YAP nuclear localization, we also used Cytochalasin D (Cyto-D) to depolymerize F-actin. Cells were pretreated with a cell culture medium containing 1 μM Cyto-D for 60 min. The control group was treated with a dimethyl sulfoxide (DMSO)-added medium.

2.6. Chromatin Remodeling and Histone Lysine Acetylation with YAP Functionalization. Chromatin remodeling and histone lysine acetylation are important for transcription factor activity, such as YAP.[33,34] To investigate chromatin remodeling, we used immunofluorescence staining and heat maps of the DAPI and qRT-PCR assays. The immunofluorescence staining procedure and qRT-PCR were the same as above. The primary antibodies used in this study are listed in Table S2. In particular, histone lysine acetylation is important for chromatin remodeling and gene expression. To investigate the association between lysine histone acetylation and YAP function

https://doi.org/10.1021/acsami.5c03093
ACS Appl. Mater. Interfaces 2025, 17, 30559−30572

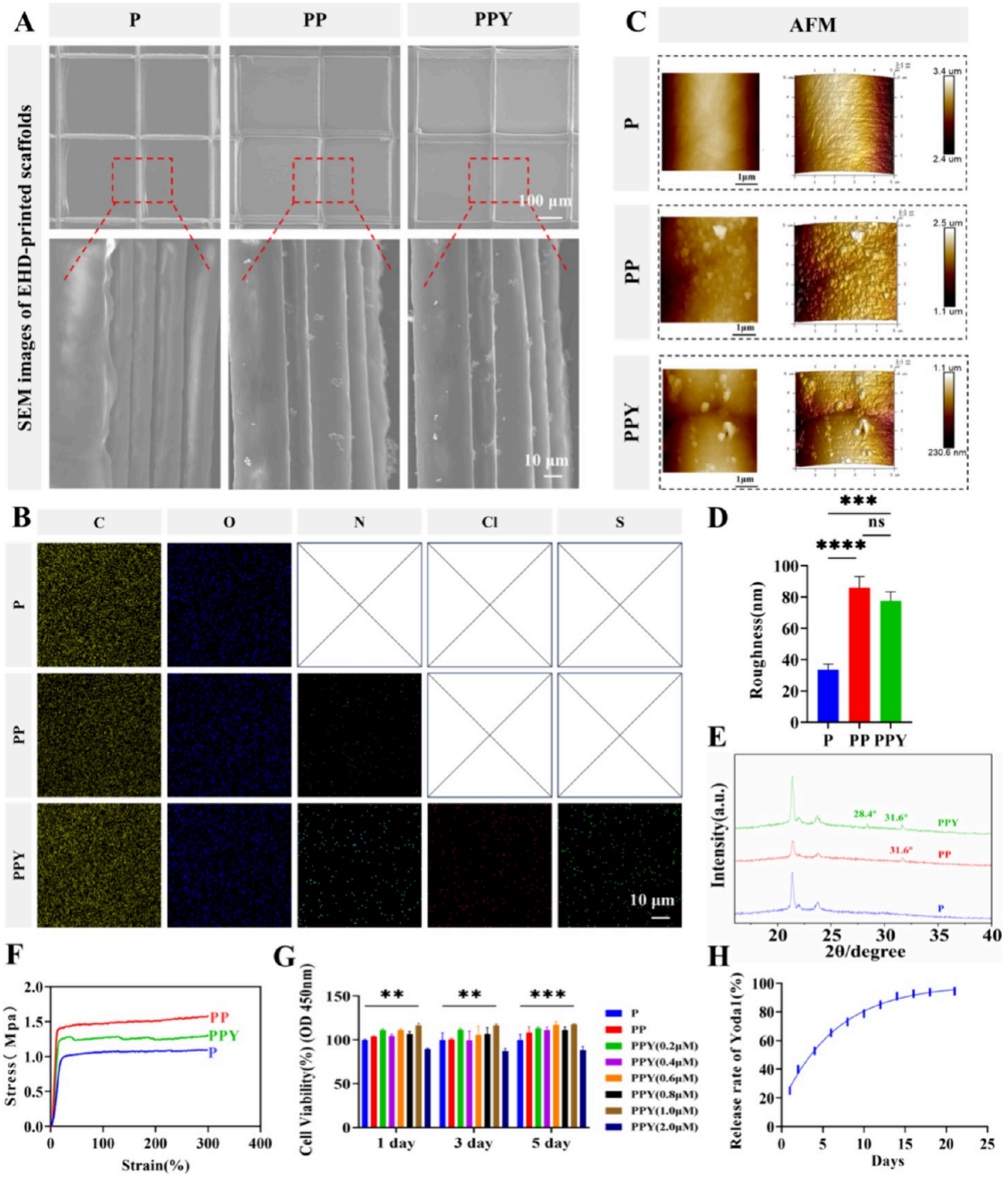

Figure 2. Characterization of EHD-printed microfibrous scaffolds. (A) SEM images of the P, PP, and PPY groups. (B) EDS elemental maps of carbon (C), oxygen (O), nitrogen (N), chlorine (Cl), and sulfur (S) in the P, PP, and PPY groups. (C) Quantitative surface morphology and (D) roughness analysis of the P, PP, and PPY groups. (E) XRD analysis of the P, PP, and PPY groups. (F) Tensile stress−strain curves of the P, PP, and PPY groups. (G) Proliferation of MC3T3-E1 cells under different concentrations of Yoda1. (H) Release curves of Yoda1 from the PPY groups. $n = 3$. $^{**}P < 0.01$, $^{***}P < 0.001$, and $^{****}P < 0.0001$.

exertion, cells were pretreated with a C646 medium configured at a concentration of 10 μM for 8 h. Also, cells pretreated with the same medium with the addition of DMSO were used as the control group. The C646 could inhibit histone lysine acetylation. Additionally, the expression levels of Piezo1, Lamin A/C, and COL-I were quantified by using qRT-PCR.

2.7. Animal Experiments. All animal procedures were approved by the Animal Research Committee of Xi'an Jiaotong University and were performed according to its guidelines. Forty-eight male Sprague−Dawley (SD) rats were selected and randomly divided into four groups: the control group, P group, PP group, and PPY group, with 12 rats in each group. After anesthesia with 1% pentobarbital (30 mg/kg), the hair on the top of the head of the rats was removed, and the rats were fixed. An incision was made on the extension of the midline to expose the cranium, and then the opening was positioned according to the location of the medial canthus of the rat and the middle cranial suture. A defective area with a diameter of 8 mm was created through the opening position using an 8 mm ring drill. Then the P, PP, and PPY groups were implanted with the pure PCL scaffolds, PDA-coated PCL scaffolds, and PDA-coated and Yoda1-loaded PCL scaffolds, respectively. The control group was left untreated. All animal wounds were closed layer by layer. Eighty thousand units of penicillin were injected within 3 days after surgery to prevent infection. Rats were executed at 4 and 12 weeks after implantation, and cranial specimens with the microfibrous scaffolds were taken and collected for further study ($n = 6$ per group).

https://doi.org/10.1021/acsami.5c03093
ACS Appl. Mater. Interfaces 2025, 17, 30559−30572

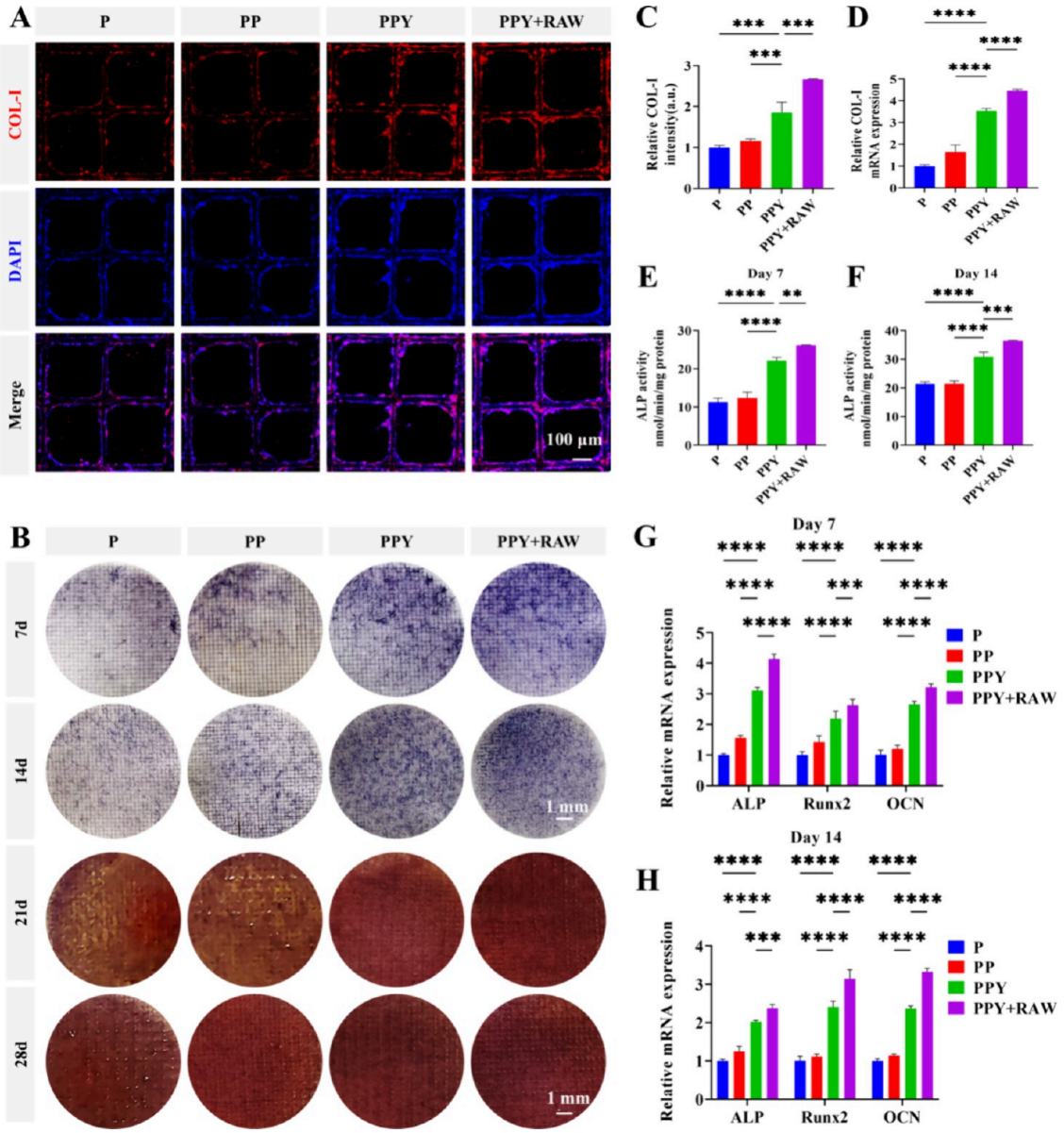

Figure 3. Osteogenic differentiation of MC3T3-E1 cells on scaffolds. (A) COL-I immunofluorescence staining and (C) semiquantitative analysis of the P, PP, PPY, and PPY+RAW groups. (B) ALP at 7 days and 14 days and ARS staining images at 21 days and 28 days of the P, PP, PPY, and PPY +RAW groups. (D) Gene expression levels of COL-I in the P, PP, PPY, and PPY+RAW groups. (E) ALP activity of the P, PP, PPY, and PPY+RAW groups at 7 days. (F) ALP activity of the P, PP, PPY, and PPY+RAW groups at 14 days. (G) ALP, Runx2, and OCN gene expression levels of the P, PP, PPY, and PPY+RAW groups at 7 days. (H) ALP, Runx2, and OCN gene expression levels of the P, PP, PPY, and PPY+RAW groups at 14 days. $n = 3$. $^{**}P < 0.01$, $^{***}P < 0.001$, and $^{****}P < 0.0001$.

2.8. Micro-CT Analysis. Cranial specimens with the microfibrous scaffolds were collected, cleaned, and fixed in 10% formalin. Subsequently, Micro-CT was used for analysis, and a cylinder with a diameter of 8 mm and a height of 2 mm was selected to be defined as the region of interest (ROI). The tube voltage and tube current were 80 kV and 0.06 mA, respectively. Bone formation was evaluated by calculating bone volume (BV), bone volume to tissue volume (BV/TV), bone mineral density (BMD), and trabecular thickness (Tb.Th) according to the previous literature.[24]

2.9. Histological Analysis. All cranial specimens were decalcified, and embedded sections were made. Immunofluorescence staining was performed to analyze the phenotype of macrophages in the defect area. Immunohistochemical (IHC) staining was performed on 4 and 12 week tissues coincubated with tumor necrosis factor-α (TNF-α) and interleukin-10 (IL-10) for analysis. To analyze new bone formation and bone maturation, according to the instructions, the histological sections were stained with hematoxylin-eosin (HE) and Masson's trichrome (Baso, China). Additionally, IHC staining was performed on tissues coincubated with COL-I and OCN for analysis. The ImageJ was used to quantify the TNF-α, IL-10, COL-I, and OCN expression in the samples.

2.10. Statistical Analysis. Unless otherwise specified, all experiments were independently repeated at least three times. All data are expressed as mean ± standard deviation. Two-tailed Student' s t test was used to compare the difference between the two groups. One-way ANOVA with Tukey' s test was performed for comparisons between three or more groups. A p-value <0.05 was considered statistically different.

3. RESULTS

3.1. Characterization of EHD-Printed Microfibrous Scaffolds Loaded with Yoda1. Figure 2A reveals that the EHD-printed PCL scaffolds had a well-organized structure with

https://doi.org/10.1021/acsami.5c03093
ACS Appl. Mater. Interfaces 2025, 17, 30559−30572

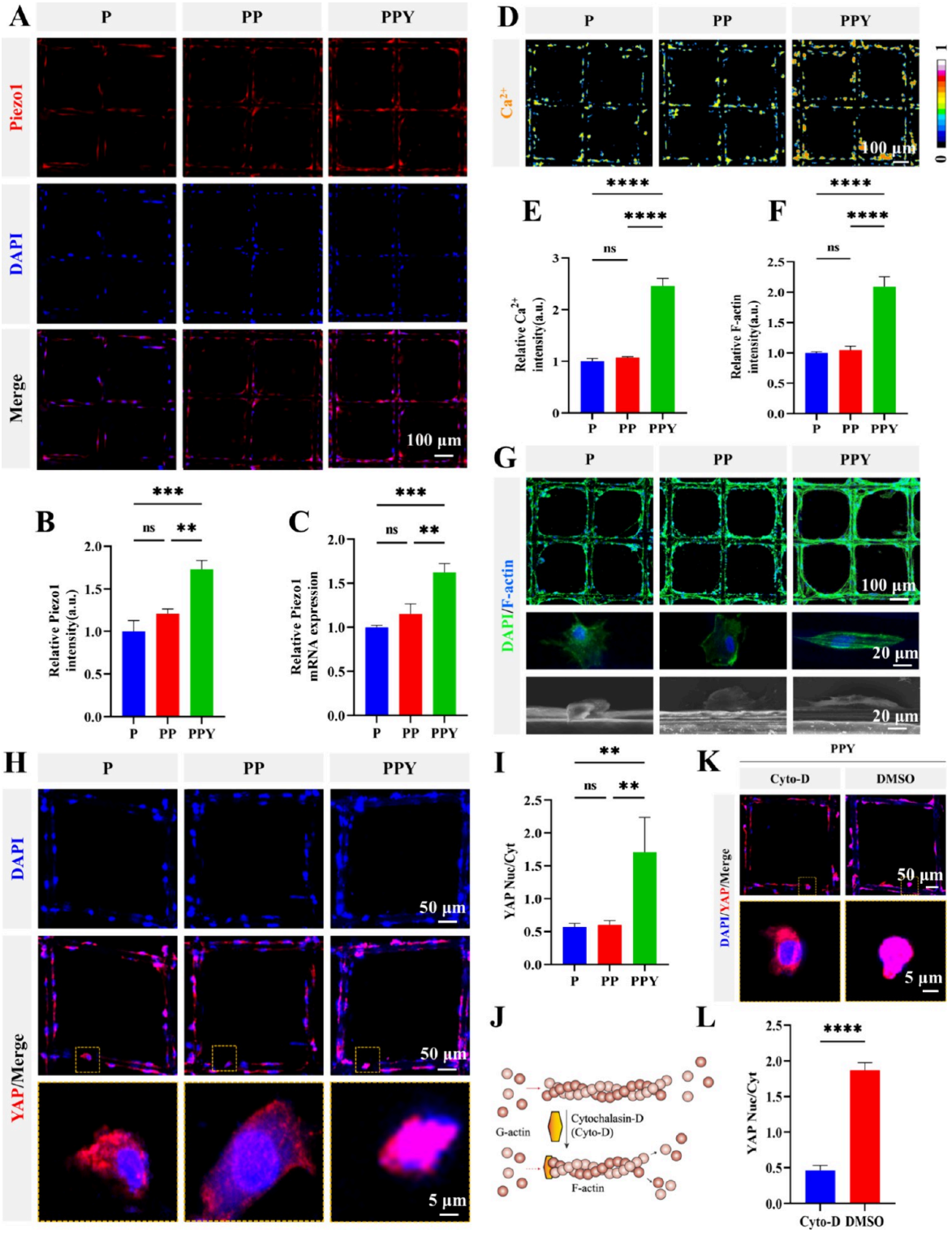

Figure 4. Yoda1-loaded scaffolds mediate YAP nuclear localization through the Piezo1-F-actin pathway. (A) Immunofluorescence staining and (B) semiquantitative analysis of Piezo1 in the P, PP, and PPY groups. (C) Piezo1 gene expression level in the P, PP, and PPY groups. (D) Immunofluorescence staining and (E) semiquantitative analysis of Ca^{2+} in the P, PP, and PPY groups. (F) Semiquantitative analysis of F-actin in the P, PP, and PPY groups. (G) Immunofluorescence staining, SEM images of F-actin in the P, PP, and PPY groups. (H) Immunofluorescence staining and (I) semiquantitative analysis of YAP in the P, PP, and PPY groups. (J) Schematic diagram of Cyto-D depolymerization of F-actin. (K) Immunofluorescence staining and (L) semiquantitative analysis of YAP in the PPY group treated with Cyto-D or DMSO. $n = 3$. $^{**}P < 0.01$, $^{***}P < 0.001$, and $^{****}P < 0.0001$.

a fiber spacing of 300 ± 16.12 μm and fiber diameters of around 30 ± 1.63 μm. The surface of the pure PCL scaffolds exhibited a smooth texture, whereas, upon treatment with PDA and Yoda1, they underwent a transformation characterized by the deposition of fine nanoparticles. The surface morphology of the scaffolds from the P, PP, and PPY groups was then assessed

https://doi.org/10.1021/acsami.5c03093
ACS Appl. Mater. Interfaces 2025, 17, 30559−30572

via AFM, showing that the scaffolds from the PP and PPY groups had significantly rougher surfaces compared to the smooth scaffolds from the P group (Figure 2C,D). The elemental composition of these scaffolds was further analyzed using EDS. Elements specific to Yoda1 small molecules, namely, chlorine (Cl) and sulfur (S), were detected in the PPY group. Nitrogen (N), a constituent element of PDA, was detected in the PP and PPY groups, while none of these elements were detected in the P group (Figure 2B and Figure S1). XRD results further confirmed our findings. A characteristic peak at 24.8° was observed in the pure PCL scaffolds. Following PDA loading, a new peak appeared at 31.6°, indicative of PDA's presence. After loading with Yoda1, a characteristic peak appeared at 28.4° (Figure 2E), which appeared to be caused by a leftward shift of the 31.6° peak after the formation of the conjugate between PDA and Yoda1.[35,36] These results demonstrate the successful loading of Yoda1 onto the PCL scaffolds. Moreover, previous studies have reported that the PDA coating improves the mechanical properties of the Nanohydroxylapatite (nano-HAP)/PCL composite scaffold.[37] In this study, the PDA coating and Yoda1-loading were also found to have some enhancement in the mechanical properties of the EHD-printed microfibrous scaffolds (Figure 2F).

The optimal loading concentration of Yoda1 was determined by CCK-8, and it was found that a loading concentration of 1 μM had a significant positive effect on cell viability compared with the others (Figure 2G and Figure S2). Therefore, 1 μM Yoda1 was used for all subsequent experiments. Live/dead staining, cell spreading area, and spreading rate further confirmed this observation, as the results demonstrated the high viability of cells seeded on the P, PP, and PPY groups (Figures S3−S5). Additionally, we quantified the expression of vinculin protein, a crucial adhesion protein in cells, across the three groups (Figures S6 and S7). Following PDA treatment, the scaffolds exhibited enhanced cell adhesion properties, with significantly higher levels of the vinculin protein observed in both PP and PPY groups compared to the P group. Furthermore, this increase in the protein content was accompanied by improved gene expression levels (Figure S8).

Afterward, we measured the release of the Yoda1 drug on the scaffolds of the PPY group. As shown in Figure 2H, Yoda1 was released more than 80% uniformly in the first 2 weeks, which is very favorable for early bone defect repair. Also, it was able to maintain sustained release for at least 21 days *in vitro*, which allowed Yoda1 to function for a longer period of time. This substantially increased the drug presence time compared to the nanocarrier delivery of Yoda1, which was only able to maintain an effective time of 12h, as fabricated by Guan et al.[38]

3.2. Osteogenic Differentiation of MC3T3-E1 on EHD-Printed Microfibrous Scaffolds. COL-I is a major organic component of the bone matrix and can be synthesized and secreted by osteoblasts during early bone regeneration.[23] As shown in Figure 3A, the Yoda1-loaded scaffolds of the PPY group showed significantly higher COL-I deposition, with the semiquantified results showing 1.85-fold higher COL-I fluorescence intensity than that of the P group. After adding supernatants of Yoda1-loaded scaffolds cocultured with RAW 264.7 cells, COL-I deposition became more abundant in the PPY+RAW group compared with the PPY group (Figure 3A,C). We performed qPCR to assess the changes in COL-I gene expression levels, which were the same as the protein expression trend with higher levels in the PPY and PPY+RAW groups (Figure 3D). Similar phenomena have also been reported in previous studies, demonstrating the ability of Yoda1 to enhance osteogenic factor secretion by RAW 264.7 cells.[16]

ALP is a marker of early osteogenesis and has a very important role in the formation of hydroxyapatite crystals in the bone matrix.[17] Our results indicated significantly deeper staining in the PPY and PPY+RAW groups compared to the other two groups at both 7 and 14 days (Figure 3B). ALP protein activity was also measured (Figure 3E,F), and the PPY and PPY+RAW groups were 22.16 ± 0.84 and 26.15 ± 0.07 nmol/min/mg protein compared to that of the P and PP groups (11.26 ± 1.03 and 12.34 ± 1.53 nmol/min/mg protein, respectively).

As shown in Figure 3B, the PPY and PPY+RAW groups showed higher calcium deposition than the other groups on days 21 and 28. In addition, we performed qPCR for the analysis of the ALP, Runx2, and OCN gene expression levels. Consistent with the previous results, the osteogenic differentiation ALP, Runx2, and OCN genes in the PPY group were significantly increased by 2−4-fold compared to the P group at days 7 and 14 (Figure 3G,H). Furthermore, the expression of ALP, Runx2, and OCN genes was also promoted in the PDA-coated PP group compared with the P group, which may be attributed to the ability of PDA to enhance the hydrophilicity and surface roughness of the scaffolds, thereby improving the osteogenic microenvironment.[28] These results suggest that PCL scaffolds loaded with Yoda1 by PDA can synergistically promote osteogenic differentiation, and this osteogenic capacity was enhanced by the addition of the RAW 264.7 cell extract to the culture medium.

3.3. Yoda1-Loaded Scaffolds Mediate YAP Nuclear Localization through the Piezo1-F-Actin Pathway. The PPY group had the highest amount of Piezo1 protein, with the semiquantified results showing 1.73-fold higher Piezo1 fluorescence intensity than that on the P group (Figure 4A,B), and the gene expression level of Piezo1 in the PPY group was found to be 1.63-fold higher than that of the P group by qPCR detection (Figure 4C). Considering that Piezo1 is a Ca^{2+} permeable cation channel, we investigated the intracellular and extracellular Ca^{2+} concentrations to ascertain the activation of Piezo1 channels. Notably, the cytoplasmic region of MC3T3-E1 cells attached to the scaffolds of the PPY group exhibited the highest intensity of Ca^{2+} fluorescence (Figure 4D,E), indicating that Piezo1 channels were indeed open.

Previous studies have demonstrated that the activation of Piezo1 induces alterations in cell membrane tension and establishes a structural connection between the cytoskeleton and Piezo1.[39] We proceeded to investigate the alterations in the cellular morphology and cytoskeletal architecture after Piezo1 activation in MC3T3-E1 cells. The expression of F-actin in cells on the scaffolds was observed to be increased in the PPY group, exhibiting a 2.1-fold higher level compared with that in the P group. This finding suggests an enhanced cytoskeleton polymerization following the Piezo1 channel activation. Moreover, the cytoskeleton morphology on the scaffolds of the PPY group was found to rearrange along the EHD-printed microfibers. Similarly, scanning electron microscopy showed that the ratio of the long to the short axis of the MC3T3-E1 cells on the scaffolds of the PPY group was higher than those of the other two groups, and the cells were more elongated (Figure 4F,G). These results suggest that Yoda1-loaded scaffolds can activate Piezo1 on MC3T3-E1 cells to promote F-actin polymerization and alter the cell morphology. Previous studies have shown that the F-actin was associated with osteogenic differentiation.[40]

https://doi.org/10.1021/acsami.5c03093
ACS Appl. Mater. Interfaces 2025, 17, 30559−30572

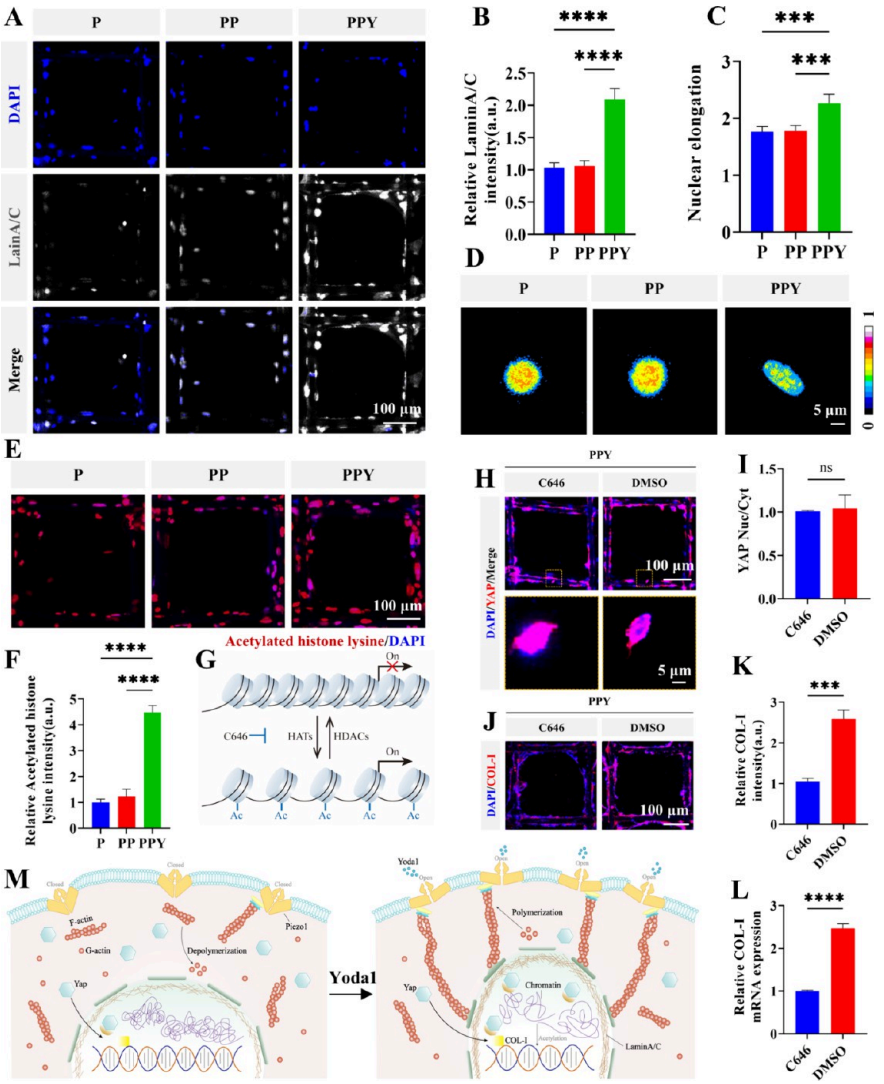

Figure 5. Chromatin remodeling and lysine acetylation mediated by Piezo1 were necessary for the exercise of YAP functions. (A) Immunofluorescence staining of LaminA/C and (B) semiquantitative analysis in the P, PP, and PPY groups. (C) Nuclear elongation quantitative analysis. (D) Heatmap showing chromatin organization in the nucleus of MC3T3-E1 cells in the P, PP, and PPY groups. (E) Immunofluorescence staining and (F) semiquantitative analysis of acetylated histone lysine in the P, PP, and PPY groups. (G) Schematic diagram of C646 inhibition of lysine acetylation. (H) YAP immunofluorescence staining and (I) semiquantitative analysis of the PPY group treated with C646 or DMSO. (J) Immunofluorescence staining and (K) semiquantitative analysis of COL-I in the PPY group treated with C646 or DMSO. (L) Gene expression level of the COL-I in the PPY group treated with C646 or DMSO. (M) Schematic diagram of Yoda1 activating Piezo1 to promote COL-I expression. $n = 3$. ***$P < 0.001$ and ****$P < 0.0001$.

To further investigate the impact of the Piezo1-F-actin pathway on osteogenic differentiation, we examined alterations in the YAP protein, a transcription factor involved in responding to regulating bone formation, which enters the nucleus before it can exert transcriptional activity.[41] The results showed that the MC3T3-E1 cells on the scaffolds of the PPY group had significantly more YAP in the nucleus, and the nucleus-to-cytoplasmic ratio (Nuc/Cyt ratio) reached 1.71 ± 0.26, compared with 0.57 ± 0.03 in the P group (Figure 4H,I). Subsequently, to verify the role of cytoskeletal polymerization in the secretion and location of YAP, we treated MC3T3-E1 cells with Cyto-D (Figure 4J). It was found that the YAP entry into the nucleus was significantly reduced in cells on the scaffold compared with the group not treated with Cyto-D (Figure 4K,L). These findings suggest that the nuclear localization of YAP in cells on the PPY group is mediated by F-actin.

3.4. Chromatin Remodeling and Lysine Acetylation Mediated by Piezo1 Were Necessary for the Exercise of YAP Functions. The F-actin not only regulates the nuclear localization of YAP but also connects with the nucleus to influence chromatin opening and transcription factor function.[34] LaminA/C, a component of the nuclear lamina, is structurally associated with F-actin.[42] The morphology of the nucleus as well as the opening of the chromatin can be observed by staining for the LaminA/C protein.[43] Our results indicated a significant increase in LaminA/C expression in the PPY group, with the semiquantified results showing 2.09-fold higher fluorescence intensity than that in the P group (Figure 5A,B and Figure S9). Additionally, the nuclei in the PPY group were more elongated, and the ratio of the long axis to the short axis of the nucleus was higher than those in the P and PP groups (Figure 5C). Previous studies have shown that increased LaminA/C expression and nuclear elongation can promote chromatin opening.[44] More-

https://doi.org/10.1021/acsami.5c03093
ACS Appl. Mater. Interfaces 2025, 17, 30559−30572

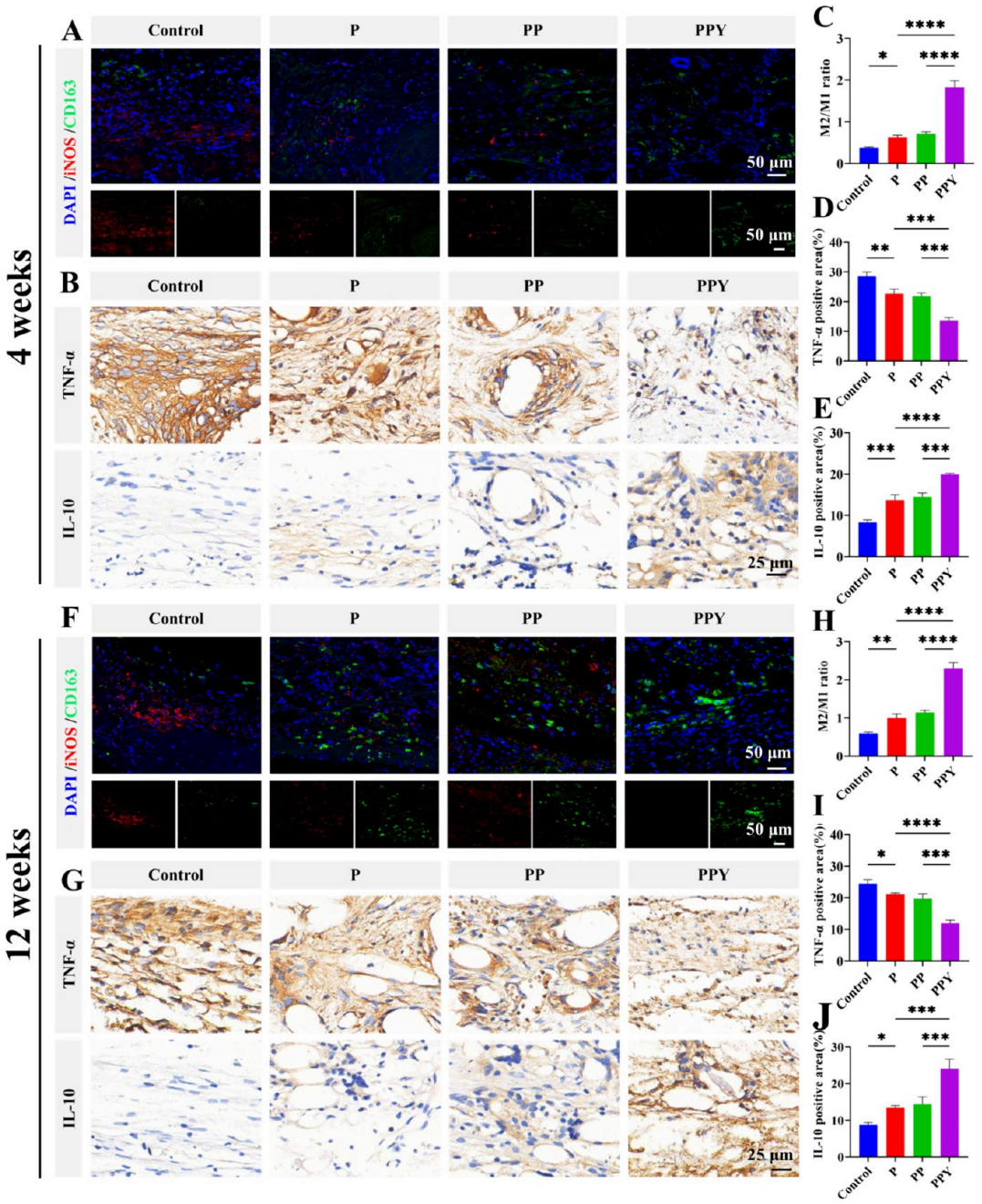

Figure 6. Macrophage phenotypic switching in the bone defect model. (A) Immunofluorescence staining images 4 weeks after stent implantation in the control, P, PP, and PPY groups: red (iNOS: M1 marker), green (CD163: M2 marker). (B) Immunochemical staining of the control, P, PP, and PPY groups of stent implantation 4 weeks after stent implantation images. (C) M2/M1 ratio 4 weeks after stent implantation in the control, P, PP, and PPY groups. (D) Percentage of positive areas for TNF-α and (E) IL-10 4 weeks after stent implantation in the control, P, PP, and PPY groups. (F) Immunofluorescence staining images 12 weeks after stent implantation in the control, P, PP, and PPY groups. (G) Immunochemical staining images 12 weeks after stent implantation in the control, P, PP, and PPY groups. (H) M2/M1 ratio 12 weeks after stent implantation in the control, P, PP, and PPY groups. (I) Percentage of positive areas for TNF-α and (J) IL-10 12 weeks after stent implantation in the control, P, PP, and PPY groups. $n = 6$. *P < 0.05, **P < 0.01, ***P < 0.001, and ****P < 0.0001.

over, we detected the nuclei with DAPI and converted the fluorescent images into visualized heat maps. The PPY group showed the lowest DAPI intensity, which indicates the loosest chromatin organization (Figure 5D). These results suggest that the Yoda1-loaded scaffolds can promote cellular chromatin opening.

Furthermore, the histone lysine acetylation is not only capable of chromatin opening but is also one of the important markers of its opening, which promotes gene expression.[45] Histone acetylation was notably higher in the PPY group compared to those in the other groups (Figure 5E,F). To investigate the effect of histone acetylation on gene expression, we treated the cells with C646,[34] an acetyltransferase inhibitor that blocks histone lysine acetylation. C646 was dissolved in DMSO prior to use, and a DMSO-only treatment was included as the control group (Figure 5G). There was no significant difference in intranuclear or cytoplasmic YAP levels between the C646 and DMSO groups (Figure 5H,I). However, at this time, it was found that after

https://doi.org/10.1021/acsami.5c03093
ACS Appl. Mater. Interfaces 2025, 17, 30559−30572

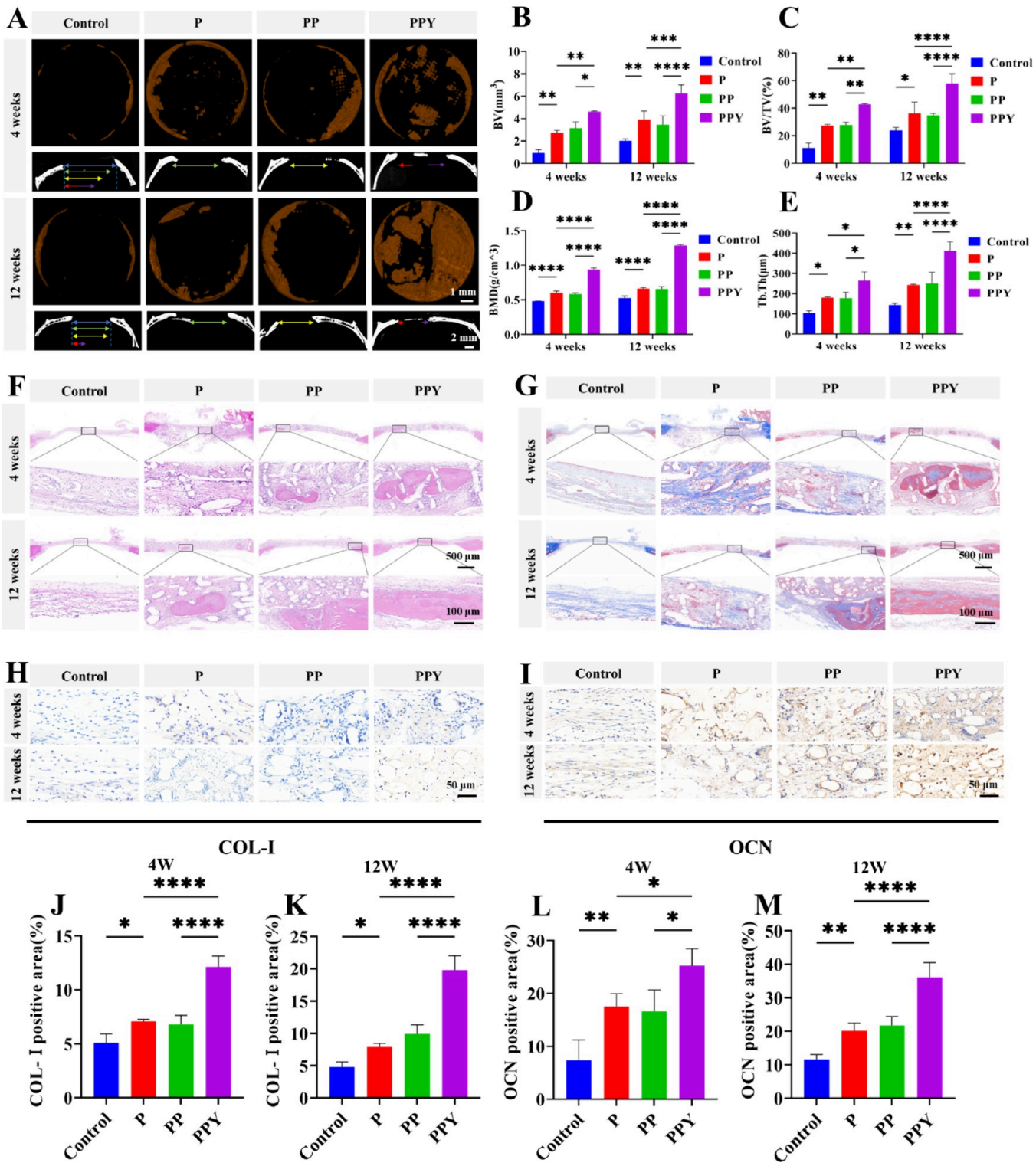

Figure 7. Bone regeneration of Yoda1-loaded scaffolds *in vivo*. (A) 3D-reconstructed images and sagittal positional maps in the control, P, PP, and PPY groups at 4 and 12 weeks. (B–E) Quantitative analysis of BV, BV/TV, BMD, and Tb.Th in the control, P, PP, and PPY groups at 4 and 12 weeks. (F) HE staining images in the control, P, PP, and PPY groups at 4 and 12 weeks. (G) Masson staining in the control, P, PP, and PPY groups at 4 and 12 weeks. (H, I) Immunochemical staining images in the control, P, PP, and PPY groups at 4 and 12 weeks. (J, K) Percentage of COL-I positive areas in the control, P, PP, and PPY groups at 4 and 12 weeks. (L, M) Percentage of the OCN positive areas in the control, P, PP, and PPY groups at 4 and 12 weeks. $n = 6$. $^{*}P < 0.05$, $^{**}P < 0.01$, $^{***}P < 0.001$, and $^{****}P < 0.0001$.

C646 treatment, COL-I protein expression was reduced, and its mRNA level also showed a significant decrease—to approximately 40% of that observed in the DMSO-treated group (Figure 5J–L). This suggests that the promotion of COL-I gene expression after YAP entry into the nucleus requires the mediation of lysine histone acetylation.

These findings suggest that the Yoda1-loaded scaffolds activate Piezo1 channels and promote increased F-actin

https://doi.org/10.1021/acsami.5c03093
ACS Appl. Mater. Interfaces 2025, 17, 30559–30572

polymerization in MC3T3-E1 cells, altering the cellular and nuclear morphology and promoting chromatin opening. At the same time, the Yoda1-loaded scaffolds were able to promote increased YAP entry into the nucleus, but the promotion of COL-I gene expression after YAP entry required the involvement of Piezo1-mediated histone lysine acetylation (Figure 5M).

3.5. Macrophage Phenotypic Switching in the Bone Defect Model. We have previously demonstrated *in vitro* that the addition of Yoda1-loaded scaffolds cocultured with macrophage supernatants can further enhance osteogenic capacity. Here, we further explored the effect of macrophages on osteointegration *in vivo*. We established a critical bone defect model, collected specimens at designated time points, and differentiated between M1 and M2 macrophages using iNOS and CD163 labeling, respectively (Figure 6A,F). The PPY group showed the fewest M1 macrophages and most M2 macrophages compared with the P and PP groups. We then performed quantitative analysis of their distribution. The ratio of M2/M1 cells was slightly higher in the PP group compared with that in the P group, but there was no statistical difference. However, the ratio of M2/M1 cells in the scaffolds of the PPY group was 2−3-fold higher than that in the P group (Figure 6C,H). This indicated that the PPY group was able to promote the polarization of the M2 macrophages *in vivo*.

Previous studies have shown that cytokines secreted by macrophages can influence bone repair.[46] Further immunohistochemical staining showed that, at 4 weeks, the PPY group produced less of the pro-inflammatory cytokine TNF-α and more of the anti-inflammatory cytokine IL-10 compared to the other two groups (Figure 6B,D,E). At 12 weeks, the same trend was observed (Figure 6G,I,J). TNF-α has been reported to be an unfavorable factor in the bone repair process, IL-10 on the contrary.[47] These results suggest that Yoda1-loaded scaffolds can improve the immune microenvironment around bone defects and facilitate the repair of bone defects.

3.6. Bone Regeneration of the Yoda1-Loaded Scaffolds *In Vivo*. To evaluate the effect of the three groups of fiber scaffolds on bone regeneration in the bone defect model, we performed 3D micro-CT reconstruction and histological analysis. The 3D CT reconstructions at 4 and 12 weeks revealed that the control group, which utilized an 8 mm scaffold, showed minimal new bone formation, indicating that self-healing is insufficient for critical-sized bone defects. In contrast, the PPY group demonstrated the greatest extent of new bone formation and exhibited superior bone regeneration efficiency compared to those of the P and PP groups. Further confirmation through 2D sagittal CT images revealed that the PPY group had the shortest bone defect lengths (Figure 7A). Quantitative analysis was performed and found that at both 4 and 12 weeks, the PPY group exhibited higher BV and BV/TV and also had the highest BMD and Tb.Th (Figure 7B−E).

Subsequently, we evaluated bone regeneration through HE and Masson staining. The HE staining results at 4 and 12 weeks showed different degrees of osteogenesis in all three groups with scaffolds; however, osteogenesis was not evident in the P and PP groups, and significant new bone formation was observed in the PPY group (Figure 7F). In particular, at 12 weeks, HE staining showed that new bone in the PPY group essentially filled the entire defect area. Then, Masoon staining was performed to verify bone maturation, and at both 4 and 12 weeks, the PPY group exhibited the highest bone formation compared with the P and PP groups (Figure 7G).

Moreover, since both COL-I and OCN are osteogenic markers, we performed IHC staining and analyzed them statistically. The results showed that at 4 and 12 weeks, the PPY group had more COL-I and OCN formation compared to the P and PP groups, which resulted in more surface bone formation (Figure 7H−M). Altogether, our study demonstrated that the Yoda1-loaded scaffolds of the PPY group were able to significantly promote the regenerative repair capacity of the bone defect areas.

4. DISCUSSION

Critical bone defects often cannot heal or repair spontaneously and require external interventions, such as tissue-engineered bone solutions.[48] In recent years, Yoda1 has been recognized as a specific activator of Piezo1 channels, capable of lowering the threshold for Piezo1 channel opening.[11,49,50] Previous studies have shown that the administration of Piezo1 agonists to adult mice increases the expression of bone formation markers and that Yoda1 treatment has been shown to accelerate fracture healing.[51] However, Wu et al. showed that high concentrations of Yoda1 may overactivate Piezo1 to accelerate nucleus pulposus cellular senescence and intervertebral disc degeneration (IDD) progression.[52] Therefore, such systemic administration of a high concentration may exist and will have other adverse effects. In our study, we found that the IC50 of Yoda1 on osteoblasts was 15.32 μM, which is similar to the study of Yang et al.[18] Moreover, we found that the biosafety was good at a concentration of 1 μM by CCK-8 and dead/live staining, which provides a concentration reference for the future application of Yoda1. Furthermore, we controlled the fiber diameter to be around 30 ± 1.63 μm by EHD printing and then loaded Yoda1 by PDA coating. Yoda1 was not directly incorporated into the biomaterial ink prior to printing, primarily because it is a small, hydrophobic molecule with limited stability under the high-pressure conditions required for EHD printing.[11] Additionally, PDA enabled the effective loading of Yoda1 while also enhancing the hydrophilicity and surface roughness of the scaffold, thereby further promoting an osteogenic microenvironment.[28] This differs from He et al. who used hydrogel loading of exosomes from BMSCs treated with Yoda1 in advance[17] and Yang et al. who prepared Yoda1-loaded bilayers using electrostatic spinning.[18] In the study, the PCL scaffolds were printed by EHD and loaded with Yoda1 drug by PDA to provide a 3D growth environment for cells, which was a simple and economical method (Table S3).

To further investigate the mechanism by which Yoda1 promotes osteogenesis. Many previous studies have pointed out the correlation between Piezo1 and YAP, such as Zhou et al.'s study that showed that Piezo1 protein levels correlate with YAP activity.[53] Recently, Guan et al. demonstrated *in vivo* that Piezo1 improves bone formation through YAP/β-catenin colocalization.[38] Zhong et al. showed that Yoda1 activates Piezo1 and thus promotes YAP activation, regulates GSL1-mediated glutamine catabolism, and enhances valvular interstitial cell (VIC) osteogenic differentiation.[54] Moreover, Kim et al. found that Piezo1 is structurally coupled to F-actin, and that a change in the conception of Piezo1 can lead to changes in cell membrane tension, which in turn leads to changes in intracellular stress.[55] Additionally, other research has indicated that there is a structural link between the nucleus and cytoskeleton through the nuclear lamina and junctions of the LINC complex.[56] In this study, we observed that the addition of Yoda1 increased YAP into the nucleus of cells and also increased

https://doi.org/10.1021/acsami.5c03093
ACS Appl. Mater. Interfaces 2025, 17, 30559−30572

the polymerization of the cytoskeleton. It was also observed that Piezo1 activation was accompanied by changes in cellular morphology with intracellular stress tending in a certain direction and elongated nuclei. However, when Cyto-D was added, which induced F-actin depolymerization, YAP entry into the nucleus was significantly reduced. These results suggest that Yoda1 can activate the Piezo1-F-actin pathway to mediate the entry of YAP into the nucleus. In addition, the transcriptional function of YAP upon its entry into the nucleus requires the mediation of lysine acetylation. Previous studies have shown that changes in cellular or nuclear morphology affect lysine acetylation, which is important for chromatin depolymerization and expression of target genes.[34,45] We found an increase in lysine histone acetylation in cells upon the addition of Yoda1. However, when C646, an inhibitor of histone acetylation, was added, YAP entry into the nucleus was still increased, but YAP transcriptional activity was not inhibited, and COL-I gene expression was reduced. Therefore, in this study, we found that Yoda1 activates Piezo1 to promote F-actin polymerization, which affects cellular and nuclear morphology, resulting in an increase in YAP incorporation into the nucleus, and at the same time, the altered nuclear morphology promotes lysine histone acetylation to mediate YAP function and affects the expression of osteoblastic gene COL-I.

Moreover, bone immune homeostasis is important for bone integration. Previous studies have indicated that Piezo1 can mediate macrophage M2 polarization and promote osteogenesis; however, it has only been experimentally validated *in vitro*.[16] In the field of tissue engineering, studies on Yoda1 are limited to osteogenesis and angiogenesis, and no studies have considered the effects of Yoda1 on the immune microenvironment and inflammatory response *in vivo*.[17,18] In this study, we found that macrophage extracts cultured with Yoda1 accelerated osteogenesis *in vitro*. Moreover, in the bone defect model, the Yoda1-loaded scaffolds of the PPY group were found to promote macrophage M2 polarization and reduce M1 polarization. Also, the production of anti-inflammatory factor IL-10 was increased and the production of pro-inflammatory factor TNF-α was decreased. Finally, we verified the ability of the scaffolds of the P, PP and PPY groups for bone defect repair in an *in vivo* bone defect model, and the results showed that the PPY group had the highest number of bone formation markers and the highest amount of new bone.

Several limitations remain in the current study. Although we focused on the immune microenvironment, we only examined macrophage polarization, without investigating other immune cells such as T and B cells, which may also play roles in bone regeneration.[57−59] The mechanisms by which Yoda1 induces M2-like polarization also require further clarification through a pathway analysis. Additionally, the osteogenic potential of the scaffold alone is limited, indicating the need for *in vivo* coimplantation with cells. Importantly, the biosafety and long-term effects of Yoda1 have not been evaluated; future studies should assess its systemic toxicity, immune response, and potential for disrupting tissue homeostasis to ensure its clinical applicability. Finally, validation in larger animal models is necessary to support translational relevance.

5. CONCLUSIONS

In conclusion, this study demonstrated that scaffolds loaded with Yoda1, produced by using EHD printing, exhibit significant osteogenic effects *in vitro*. We elucidated the mechanism by which Yoda1 activates the Piezo1-F-actin pathway to mediate YAP nuclear translocation and identified lysine acetylation as crucial for YAP's functionality. *In vivo*, the PPY group was shown to modulate the bone immune microenvironment, promote macrophage M2 polarization, and have excellent osteogenic capacity. Through the elaboration of the immune microenvironment and the study of the specific osteogenic mechanism of YAP, we may be able to provide strong evidence to support clinical application of Yoda1 in the future.

■ ASSOCIATED CONTENT

Supporting Information

The Supporting Information is available free of charge at https://pubs.acs.org/doi/10.1021/acsami.5c03093.

Experimental details, additional results and characterization details including EDS images, live/dead staining images, cell area, cell spreading rate, and immunofluorescence images (PDF)

■ AUTHOR INFORMATION

Corresponding Authors

Jiankang He − *State Key Laboratory for Manufacturing Systems Engineering, National Medical Products Administration (NMPA) Key Laboratory for Research and Evaluation of Additive Manufacturing Medical Devices, and State Industry-Education Integration Center for Medical Innovations, Xi'an Jiaotong University, Xi'an 710049, P. R. China;* orcid.org/0000-0002-9386-5833; Email: jiankanghe@mail.xjtu.edu.cn

Wei Wang − *Comprehensive Orthopedics Department, the Second Affiliated Hospital of Xi'an Jiaotong University, Xi'an, Shaanxi 710004, P. R. China*; Email: dr.wangwei@xjtu.edu.cn

Authors

Junzheng Liu − *Comprehensive Orthopedics Department, the Second Affiliated Hospital of Xi'an Jiaotong University, Xi'an, Shaanxi 710004, P. R. China; State Key Laboratory for Manufacturing Systems Engineering, Xi'an Jiaotong University, Xi'an 710049, P. R. China;* orcid.org/0000-0001-6852-9697

Zijie Meng − *Frontier Institute of Science and Technology, State Key Laboratory for Manufacturing Systems Engineering, National Medical Products Administration (NMPA) Key Laboratory for Research and Evaluation of Additive Manufacturing Medical Devices, and State Industry-Education Integration Center for Medical Innovations, Xi'an Jiaotong University, Xi'an 710049, P. R. China*

Jidong Song − *Comprehensive Orthopedics Department, the Second Affiliated Hospital of Xi'an Jiaotong University, Xi'an, Shaanxi 710004, P. R. China*

Jiaming Yu − *Shaanxi University of Chinese Medicine, Xianyang, Shaanxi 712046, P. R. China*

Qin Guo − *Comprehensive Orthopedics Department, the Second Affiliated Hospital of Xi'an Jiaotong University, Xi'an, Shaanxi 710004, P. R. China*

Jiahao Zhang − *Comprehensive Orthopedics Department, the Second Affiliated Hospital of Xi'an Jiaotong University, Xi'an, Shaanxi 710004, P. R. China*

Shuo Wang − *Shaanxi University of Chinese Medicine, Xianyang, Shaanxi 712046, P. R. China*

https://doi.org/10.1021/acsami.5c03093
ACS Appl. Mater. Interfaces 2025, 17, 30559−30572

Yulin Wang − *Comprehensive Orthopedics Department, the Second Affiliated Hospital of Xi'an Jiaotong University, Xi'an, Shaanxi 710004, P. R. China*

Zhennan Qiu − *State Key Laboratory for Manufacturing Systems Engineering, National Medical Products Administration (NMPA) Key Laboratory for Research and Evaluation of Additive Manufacturing Medical Devices, and State Industry-Education Integration Center for Medical Innovations, Xi'an Jiaotong University, Xi'an 710049, P. R. China*

Xinyi Zhang − *Comprehensive Orthopedics Department, the Second Affiliated Hospital of Xi'an Jiaotong University, Xi'an, Shaanxi 710004, P. R. China*

Complete contact information is available at: https://pubs.acs.org/10.1021/acsami.5c03093

Author Contributions

†J.L. and Z.M. contributed equally to this work.

Notes

The authors declare no competing financial interest.

■ ACKNOWLEDGMENTS

This work was financially supported by the National Natural Science Foundation of China (52125501, 52405325, and 82072522), the Cross training Support Project for Doctoral Students at Xi'an Jiaotong University (IDT2315), the Key Research Project of Shaanxi Province (2021LLRH-08 and 2024SF2-GJHX-34), the Program for Innovation Team of Shaanxi Province (2023-CX-TD-17), the Postdoctoral Fellowship Program of CPSF (GZB20230573), the China Postdoctoral Science Foundation (2024M762577), the Postdoctoral Project of Shaanxi Province (2023BSHYDZZ30), the State Key Laboratory of Oral & Maxillofacial Reconstruction and Regeneration (2024KB04), and the Fundamental Research Funds for the Central Universities.

■ REFERENCES

(1) Ha, Y.; Ma, X.; Li, S.; Li, T.; Li, Z.; Qian, Y.; Shafiq, M.; Wang, J.; Zhou, X.; He, C. Bone Microenvironment-Mimetic Scaffolds with Hierarchical Microstructure for Enhanced Vascularization and Bone Regeneration. *Adv. Funct Materials* **2022**, *32* (20), No. 2200011.

(2) Qiu, S.; Cao, L.; Xiang, D.; Wang, S.; Wang, D.; Qian, Y.; Li, X.; Zhou, X. Enhanced Osteogenic Differentiation in 3D Hydrogel Scaffold via Macrophage Mitochondrial Transfer. *J. Nanobiotechnol* **2024**, *22* (1), 540.

(3) Li, X.; Han, L.; Nookaew, I.; Mannen, E.; Silva, M. J.; Almeida, M.; Xiong, J. Stimulation of Piezo1 by Mechanical Signals Promotes Bone Anabolism. *Elife* **2019**, *8*, No. e49631.

(4) Li, Z.; Chen, K.; Yu, Q.; Li, Y.; Tong, S.; Xu, R.; Hu, R.; Zhang, Y.; Xu, W. Suppression of NFATc1 through NF-kB/PI3K Signaling Pathway by Oleandrin to Inhibit Osteoclastogenesis and Bone Resorption. *Eng. Regener.* **2024**, *5* (3), 342−349.

(5) Coste, B.; Mathur, J.; Schmidt, M.; Earley, T. J.; Ranade, S.; Petrus, M. J.; Dubin, A. E.; Patapoutian, A. Piezo1 and Piezo2 Are Essential Components of Distinct Mechanically Activated Cation Channels. *Science* **2010**, *330* (6000), 55−60.

(6) Sun, W.; Chi, S.; Li, Y.; Ling, S.; Tan, Y.; Xu, Y.; Jiang, F.; Li, J.; Liu, C.; Zhong, G.; Cao, D.; Jin, X.; Zhao, D.; Gao, X.; Liu, Z.; Xiao, B.; Li, Y. The Mechanosensitive Piezo1 Channel Is Required for Bone Formation. *Elife* **2019**, *8*, No. e47454.

(7) Zhang, G.; Li, X.; Wu, L.; Qin, Y.-X. Piezo1 Channel Activation in Response to Mechanobiological Acoustic Radiation Force in Osteoblastic Cells. *Bone Res.* **2021**, *9* (1), 16.

(8) Sugimoto, A.; Miyazaki, A.; Kawarabayashi, K.; Shono, M.; Akazawa, Y.; Hasegawa, T.; Ueda-Yamaguchi, K.; Kitamura, T.; Yoshizaki, K.; Fukumoto, S.; Iwamoto, T. Piezo Type Mechanosensitive Ion Channel Component 1 Functions as a Regulator of the Cell Fate Determination of Mesenchymal Stem Cells. *Sci. Rep* **2017**, *7* (1), 17696.

(9) Song, J.; Liu, L.; Lv, L.; Hu, S.; Tariq, A.; Wang, W.; Dang, X. Fluid Shear Stress Induces Runx-2 Expression via Upregulation of PIEZO1 in MC3T3-E1 Cells. *Cell Biol. Int.* **2020**, *44* (7), 1491−1502.

(10) Xing, Y.; Yang, B.; He, Y.; Xie, B.; Zhao, T.; Chen, J. Effects of Mechanosensitive Ion Channel Piezo1 on Proliferation and Osteogenic Differentiation of Human Dental Follicle Cells. *Ann. Anat.* **2022**, *239*, No. 151847.

(11) Botello-Smith, W. M.; Jiang, W.; Zhang, H.; Ozkan, A. D.; Lin, Y.-C.; Pham, C. N.; Lacroix, J. J.; Luo, Y. A Mechanism for the Activation of the Mechanosensitive Piezo1 Channel by the Small Molecule Yoda1. *Nat. Commun.* **2019**, *10* (1), 4503.

(12) Gan, D.; Tao, C.; Jin, X.; Wu, X.; Yan, Q.; Zhong, Y.; Jia, Q.; Wu, L.; Huo, S.; Qin, L.; Xiao, G. Piezo1 Activation Accelerates Osteoarthritis Progression and the Targeted Therapy Effect of Artemisinin. *J. Adv. Res.* **2024**, *62*, 105−117.

(13) Lawrence, K. M.; Jones, R. C.; Jackson, T. R.; Baylie, R. L.; Abbott, B.; Bruhn-Olszewska, B.; Board, T. N.; Locke, I. C.; Richardson, S. M.; Townsend, P. A. Chondroprotection by Urocortin Involves Blockade of the Mechanosensitive Ion Channel Piezo1. *Sci. Rep* **2017**, *7* (1), 5147.

(14) Jiang, Y.; Song, J.; Xu, Y.; Liu, C.; Qian, W.; Bai, T.; Hou, X. Piezo1 Regulates Intestinal Epithelial Function by Affecting the Tight Junction Protein Claudin-1 via the ROCK Pathway. *Life Sci.* **2021**, *275*, No. 119254.

(15) Jiang, F.; Yin, K.; Wu, K.; Zhang, M.; Wang, S.; Cheng, H.; Zhou, Z.; Xiao, B. The Mechanosensitive Piezo1 Channel Mediates Heart Mechano-Chemo Transduction. *Nat. Commun.* **2021**, *12* (1), 869.

(16) Cai, G.; Lu, Y.; Zhong, W.; Wang, T.; Li, Y.; Ruan, X.; Chen, H.; Sun, L.; Guan, Z.; Li, G.; Zhang, H.; Sun, W.; Chen, M.; Zhang, W.; Wang, H. Piezo1-mediated M2Macrophage Mechanotransduction Enhances Bone Formation through Secretion and Activation of Transforming Growth Factor-β1. *Cell Prolif* **2023**, *56*, No. e13440.

(17) He, X.; Liu, Y.; Dai, Z.; Chen, Y.; Liu, W.; Dai, H.; Hu, Y. Yoda1 Pretreated BMSC Derived Exosomes Accelerate Osteogenesis by Activating Phospho-ErK Signaling via Yoda1-Mediated Signal Transmission. *J. Nanobiotechnol* **2024**, *22* (1), 407.

(18) Yang, J.; Yuan, K.; Zhang, T.; Zhou, S.; Li, W.; Chen, Z.; Wang, Y. Accelerated Bone Reconstruction by the Yoda1 Bilayer Membrane via Promotion of Osteointegration and Angiogenesis. *Adv. Healthcare Materials* **2023**, *12*, No. 2203105.

(19) Meng, Z.; Yang, S.; Yin, F.; Liang, X.; Yan, X.; Li, X.; He, J.; Wang, L.; Li, D. 3D-Printed Biodegradable Polycaprolactone Rib Implants with Tissue-Specific Mechanical Properties Promote Chest Wall Recovery by Stimulating Tissue Fibrosis. *Virtual. Phys. Prototyp.* **2024**, *19* (1), No. e2346816.

(20) He, J.; Xia, P.; Li, D. Development of Melt Electrohydrodynamic 3D Printing for Complex Microscale Poly (ε -Caprolactone) Scaffolds. *Biofabrication* **2016**, *8* (3), No. 035008.

(21) Hochleitner, G.; Jüngst, T.; Brown, T. D.; Hahn, K.; Moseke, C.; Jakob, F.; Dalton, P. D.; Groll, J. Additive Manufacturing of Scaffolds with Sub-Micron Filaments via Melt Electrospinning Writing. *Biofabrication* **2015**, *7* (3), No. 035002.

(22) Meng, Z.; Mu, X.; He, J.; Zhang, J.; Ling, R.; Li, D. Embedding Aligned Nanofibrous Architectures within 3D-Printed Polycaprolactone Scaffolds for Directed Cellular Infiltration and Tissue Regeneration. *Int. J. Extrem. Manuf.* **2023**, *5* (2), No. 025001.

(23) Hu, S.; Meng, Z.; Zhou, J.; Li, Y.; Su, Y.; Lei, Q.; Mao, M.; Qu, X.; He, J.; Wang, W. Enhanced Attachment and Collagen Type I Deposition of MC3T3-E1 Cells via Electrohydrodynamic Printed Sub-Microscale Fibrous Architectures. *Int. J. Bioprint* **2022**, *8* (2), 514.

(24) Shi, Y.; Tao, W.; Yang, W.; Wang, L.; Qiu, Z.; Qu, X.; Dang, J.; He, J.; Fan, H. Calcium Phosphate Coating Enhances Osteointegration of Melt Electrowritten Scaffold by Regulating Macrophage Polarization. *J. Nanobiotechnol* **2024**, *22* (1), 47.

(25) Hewitt, E.; Mros, S.; Mcconnell, M.; Cabral, J.; Ali, A. Melt-Electrowriting with Novel Milk Protein/PCL Biomaterials for Skin Regeneration. *Biomed. Mater.* **2019**, *14*, No. 055013.
(26) Kade, J. C.; Dalton, P. D. Polymers for Melt Electrowriting. *Adv. Healthcare Mater.* **2021**, *10* (1), No. 2001232.
(27) Lee, H.; Dellatore, S. M.; Miller, W. M.; Messersmith, P. B. Mussel-Inspired Surface Chemistry for Multifunctional Coatings. *Science* **2007**, *318* (5849), 426−430.
(28) Liu, Y.; Ai, K.; Lu, L. Polydopamine and Its Derivative Materials: Synthesis and Promising Applications in Energy, Environmental, and Biomedical Fields. *Chem. Rev.* **2014**, *114* (9), 5057−5115.
(29) Piccolo, S.; Dupont, S.; Cordenonsi, M. The Biology of YAP/TAZ: Hippo Signaling and Beyond. *Physiol. Rev.* **2014**, *94* (4), 1287−1312.
(30) Mo, J.; Park, H. W.; Guan, K. The Hippo Signaling Pathway in Stem Cell Biology and Cancer. *EMBO Rep* **2014**, *15* (6), 642−656.
(31) Zhao, B.; Li, L.; Lei, Q.; Guan, K. L. The Hippo-YAP Pathway in Organ Size Control and Tumorigenesis: An Updated Version. *Genes Dev.* **2010**, *24* (9), 862−874.
(32) Low, B. C.; Pan, C. Q.; Shivashankar, G. V.; Bershadsky, A.; Sudol, M.; Sheetz, M. YAP/TAZ as Mechanosensors and Mechanotransducers in Regulating Organ Size and Tumor Growth. *FEBS Lett.* **2014**, *588* (16), 2663−2670.
(33) Liu, Z.; Mao, S.; Hu, Y.; Liu, F.; Shao, X. Hydrogel Platform Facilitating Astrocytic Differentiation through Cell Mechanosensing and YAP-Mediated Transcription. *Mater. Today. Bio.* **2023**, *22*, No. 100735.
(34) Shi, N.; Wang, J.; Tang, S.; Zhang, H.; Wei, Z.; Li, A.; Ma, Y.; Xu, F. Matrix Nonlinear Viscoelasticity Regulates Skeletal Myogenesis through MRTF Nuclear Localization and Nuclear Mechanotransduction. *Small* **2024**, *20*, No. e2305218.
(35) Billinge, S. J. L.; Levin, I. The Problem with Determining Atomic Structure at the Nanoscale. *Science* **2007**, *316* (5824), 561−565.
(36) Wang, F.; Han, R.; Liu, G.; Chen, H.; Ren, T.; Yang, H.; Wen, Y. Construction of Polydopamine/Silver Nanoparticles Multilayer Film for Hydrogen Peroxide Detection. *J. Electroanal. Chem. (Lausanne).* **2013**, *706*, 102−107.
(37) Shie, M.; Fang, H.-Y.; Lin, Y.-H.; Lee, A.; Yu, J.; Chen, Y.-W. Application of Piezoelectric Cells Printing on Three-Dimensional Porous Bioceramic Scaffold for Bone Regeneration. *Int. J. Bioprint.* **2019**, *5*, 210.
(38) Guan, H.; Wang, W.; Jiang, Z.; Zhang, B.; Ye, Z.; Zheng, J.; Chen, W.; Liao, Y.; Zhang, Y. Magnetic Aggregation-Induced Bone-Targeting Nanocarrier with Effects of Piezo1 Activation and Osteogenic−Angiogenic Coupling for Osteoporotic Bone Repair. *Adv. Mater.* **2024**, *36*, No. e2312081.
(39) Yang, X.; Lin, C.; Chen, X.; Li, S.; Li, X.; Xiao, B. Structure Deformation and Curvature Sensing of PIEZO1 in Lipid Membranes. *Nature* **2022**, *604* (7905), 377−383.
(40) Janmohammadi, M.; Nourbakhsh, M. S.; Bahraminasab, M.; Tayebi, L. Enhancing Bone Tissue Engineering with 3D-Printed Polycaprolactone Scaffolds Integrated with Tragacanth Gum/Bioactive Glass. *Mater. Today. Bio.* **2023**, *23*, No. 100872.
(41) Li, Y.; Zhong, Z.; Xu, C.; Wu, X.; Li, J.; Tao, W.; Wang, J.; Du, Y.; Zhang, S. 3D Micropattern Force Triggers YAP Nuclear Entry by Transport across Nuclear Pores and Modulates Stem Cells Paracrine. *Natl. Sci. Rev.* **2023**, *10* (8), 165.
(42) Vahabikashi, A.; Sivagurunathan, S.; Nicdao, F. A. S.; Han, Y. L.; Park, C. Y.; Wong, X.; Tran, J. R.; Gundersen, G. G.; Reddy, K. L.; Luxton, G. W. G.; Guo, M.; Fredberg, J. J.; Zheng, Y.; Adam, S. A.; Goldman, R. D. Nuclear lamin isoforms differentially contribute to LINC complex-dependent nucleocytoskeletal coupling and whole cell mechanics. *Proc. Natl. Acad. Sci. U. S. A.* **2022**, *119* (17), No. e2121816119.
(43) Dupont, S.; Wickström, S. A. Mechanical Regulation of Chromatin and Transcription. *Nat. Rev. Genet* **2022**, *23* (10), 624−643.
(44) Wang, Y.; Nagarajan, M.; Uhler, C.; Shivashankar, G. V. Orientation and Repositioning of Chromosomes Correlate with Cell Geometry−Dependent Gene Expression. *MBoC* **2017**, *28* (14), 1997−2009.
(45) Bascom, G.; Schlick, T. Linking Chromatin Fibers to Gene Folding by Hierarchical Looping. *Biophys. J.* **2017**, *112* (3), 434−445.
(46) Pajarinen, J.; Lin, T.; Gibon, E.; Kohno, Y.; Maruyama, M.; Nathan, K.; Lu, L.; Yao, Z.; Goodman, S. B. Mesenchymal Stem Cell-Macrophage Crosstalk and Bone Healing. *Biomaterials* **2019**, *196*, 80−89.
(47) Schlundt, C.; Fischer, H.; Bucher, C. H.; Rendenbach, C.; Duda, G. N.; Schmidt-Bleek, K. The Multifaceted Roles of Macrophages in Bone Regeneration: A Story of Polarization, Activation and Time. *Acta Biomater.* **2021**, *133*, 46−57.
(48) Zhao, J.; Zhang, K.; Wang, L.; Zhu, Z.; Jiang, D.; Zuo, Y.; Yang, J.; Jia, W. Macrophage Intracellular "Calcium Oscillations" Triggered Through In Situ Mineralization Regulate Bone Immunity to Facilitate Bone Repair. *Adv. Funct. Mater.* **2024**, *34* (26), No. 2316224.
(49) Syeda, R.; Xu, J.; Dubin, A. E.; Coste, B.; Mathur, J.; Huynh, T.; Matzen, J.; Lao, J.; Tully, D. C.; Engels, I. H.; Petrassi, H. M.; Schumacher, A. M.; Montal, M.; Bandell, M.; Patapoutian, A. Chemical Activation of the Mechanotransduction Channel Piezo1. *Elife* **2015**, *4*, No. e07369.
(50) Lacroix, J. J.; Botello-Smith, W. M.; Luo, Y. Probing the Gating Mechanism of the Mechanosensitive Channel Piezo1 with the Small Molecule Yoda1. *Nat. Commun.* **2018**, *9* (1), 4503.
(51) Liu, Y.; Tian, H.; Hu, Y.; Cao, Y.; Song, H.; Lan, S.; Dai, Z.; Chen, W.; Zhang, Y.; Shao, Z.; Liu, Y.; Tong, W. Mechanosensitive Piezo1 Is Crucial for Periosteal Stem Cell-Mediated Fracture Healing. *Int. J. Biol. Sci.* **2022**, *18* (10), 3961−3980.
(52) Wu, J.; Chen, Y.; Liao, Z.; Liu, H.; Zhang, S.; Zhong, D.; Qiu, X.; Chen, T.; Su, D.; Ke, X.; Wan, Y.; Zhou, T.; Su, P. Self-Amplifying Loop of NF-κB and Periostin Initiated by PIEZO1 Accelerates Mechano-Induced Senescence of Nucleus Pulposus Cells and Intervertebral Disc Degeneration. *Mol. Ther.* **2022**, *30* (10), 3241−3256.
(53) Zhou, T.; Gao, B.; Fan, Y.; Liu, Y.; Feng, S.; Cong, Q.; Zhang, X.; Zhou, Y.; Yadav, P. S.; Lin, J.; Wu, N.; Zhao, L.; Huang, D.; Zhou, S.; Su, P.; Yang, Y. Piezo1/2 Mediate Mechanotransduction Essential for Bone Formation through Concerted Activation of NFAT-YAP1-ß-Catenin. *Elife* **2020**, *9*, No. e52779.
(54) Zhong, G.; Su, S.; Li, J.; Zhao, H.; Hu, D.; Chen, J.; Li, S.; Lin, Y.; Wen, L.; Lin, X.; Xian, G.; Xu, D.; Zeng, Q. Activation of Piezo1 Promotes Osteogenic Differentiation of Aortic Valve Interstitial Cell through YAP-Dependent Glutaminolysis. *Sci. Adv.* **2023**, *9* (22), No. eadg0478.
(55) Kim, J.-K.; Louhghalam, A.; Lee, G.; Schafer, B. W.; Wirtz, D.; Kim, D.-H. Nuclear Lamin A/C Harnesses the Perinuclear Apical Actin Cables to Protect Nuclear Morphology. *Nat. Commun.* **2017**, *8* (1), 2123.
(56) Leong, E. L.; Khaing, N. T.; Cadot, B.; Hong, W. L.; Kozlov, S.; Werner, H.; Wong, E. S. M.; Stewart, C. L.; Burke, B.; Lee, Y. L. Nesprin-1 LINC Complexes Recruit Microtubule Cytoskeleton Proteins and Drive Pathology in *Lmna*-Mutant Striated Muscle. *Hum. Mol. Genet.* **2023**, *32* (2), 177−191.
(57) Murayama, M.; Chow, S. K.; Lee, M. L.; Young, B.; Ergul, Y. S.; Shinohara, I.; Susuki, Y.; Toya, M.; Gao, Q.; Goodman, S. B. The Interactions of Macrophages, Lymphocytes, and Mesenchymal Stem Cells during Bone Regeneration. *Bone Joint Res.* **2024**, *13* (9), 462−473.
(58) Liu, T.; You, Z.; Shen, F.; Yang, P.; Chen, J.; Meng, S.; Wang, C.; Xiong, D.; You, C.; Wang, Z.; Shi, Y.; Ye, L. Tricarboxylic Acid Cycle Metabolite-Coordinated Biohydrogels Augment Cranial Bone Regeneration Through Neutrophil-Stimulated Mesenchymal Stem Cell Recruitment and Histone Acetylation-Mediated Osteogenesis. *ACS Appl. Mater. Interfaces* **2024**, *16* (5), 5486−5503.
(59) Ding, P.; Gao, C.; Gao, Y.; Liu, D.; Li, H.; Xu, J.; Chen, X.; Huang, Y.; Zhang, C.; Zheng, M.; Gao, J. Osteocytes Regulate Senescence of Bone and Bone Marrow. *Elife* **2022**, *11*, No. e81480.

https://doi.org/10.1021/acsami.5c03093
ACS Appl. Mater. Interfaces 2025, 17, 30559−30572